Regional and Global Impacts of Land Cover Change and Sea Surface Temperature Anomalies

KIRSTEN L. FINDELL

NOAA/Geophysical Fluid Dynamics Laboratory, Princeton, New Jersey, and Climate Change Research Centre, University of New South Wales, Sydney, New South Wales, Australia

ANDREW J. PITMAN AND MATTHEW H. ENGLAND

Climate Change Research Centre, University of New South Wales, Sydney, New South Wales, Australia

PHILIP J. PEGION*

Global Modeling and Assimilation Office, NASA Goddard Space Flight Center, Greenbelt, and Science Applications International Corporation, Beltsville, Maryland

(Manuscript received 14 April 2008, in final form 24 September 2008)

ABSTRACT

The atmospheric and land components of the Geophysical Fluid Dynamics Laboratory's (GFDL's) Climate Model version 2.1 (CM2.1) is used with climatological sea surface temperatures (SSTs) to investigate the relative climatic impacts of historical anthropogenic land cover change (LCC) and realistic SST anomalies. The SST forcing anomalies used are analogous to signals induced by El Niño–Southern Oscillation (ENSO), the North Atlantic Oscillation (NAO), and the background global warming trend. Coherent areas of LCC are represented throughout much of central and eastern Europe, northern India, southeastern China, and on either side of the ridge of the Appalachian Mountains in North America. Smaller areas of change are present in various tropical regions. The land cover changes in the model are almost exclusively a conversion of forests to grasslands.

Model results show that, at the global scale, the physical impacts of LCC on temperature and rainfall are less important than large-scale SST anomalies, particularly those due to ENSO. However, in the regions where the land surface has been altered, the impact of LCC can be equally or more important than the SST forcing patterns in determining the seasonal cycle of the surface water and energy balance. Thus, this work provides a context for the impacts of LCC on climate: namely, strong regional-scale impacts that can significantly change globally averaged fields but that rarely propagate beyond the disturbed regions. This suggests that proper representation of land cover conditions is essential in the design of climate model experiments, particularly if results are to be used for regional-scale assessments of climate change impacts.

1. Introduction

The earth's climate responds to a variety of internal and external forcing terms (Baede et al. 2001). There is very high confidence that the net effect of human activities since 1750 has caused warming and that the amount of warming is large relative to changes in solar irradiance (Forster et al. 2007). The 2001 and 2007 reports by the Intergovernmental Panel on Climate Change (IPCC) focus principally on the impact of increasing greenhouse gases, but both reports also identify other forcing terms, including land cover change.

The significance of land cover change on large-scale climate is disputed. Land cover change (LCC) alters the surface energy and moisture balances as a result of changes in rooting depth and canopy height and structure of vegetation (Findell et al. 2007). The partitioning of available energy between sensible and latent heat

* Current affiliation: NOAA/NCEP/Climate Prediction Center, Camp Springs, Maryland.

Corresponding author address: Dr. Kirsten L. Findell, Geophysical Fluid Dynamics Laboratory, 201 Forrestal Road, Princeton, NJ 08540-6649.
E-mail: kirsten.findell@noaa.gov

DOI: 10.1175/2008JCLI2580.1

fluxes is sensitive to land cover conditions, as is the partitioning of precipitation between runoff and evaporation (Pitman 2003). Removal of natural vegetation tends to decrease rooting depths, which reduces moisture availability, leading to increased sensible heat flux and warmer and deeper boundary layers. In contrast, reforestation typically increases the latent heat flux via transpiration and interception loss, which cools and moistens the boundary layer (Betts et al. 1996). These changes in the root and canopy structure of land cover are accompanied by changes in albedo, which impacts radiative forcing (Forster et al. 2007; Findell et al. 2007). The change associated with deforestation is normally a decrease in radiative forcing via an increase in albedo (hence this acts to cool the surface through the radiation balance), and the albedo increase can be amplified via a positive feedback with snow (Betts 2000). Models that emphasize the albedo change rather than the changes in available moisture predict a regional cooling associated with deforestation in the midlatitudes (e.g., Bonan 1999; Govindasamy et al. 2001; Matthews et al. 2003). However, studies that also include the changes to the partitioning of available energy tend to predict a regional warming in the midlatitudes due to deforestation (e.g., Findell et al. 2007).

The exploration of the impact of land cover change on the atmosphere is one of the oldest experiments conducted with climate models (Henderson-Sellers and Gornitz 1984). A vast literature has developed, focused on the impact of tropical deforestation (Dickinson and Henderson-Sellers 1988; McGuffie et al. 1995; Sud et al. 1996; Chase et al. 2000; Avissar and Werth 2005; Findell et al. 2006) and the impact of global LCC, including the impact of temperate deforestation (Bonan 1999; Govindasamy et al. 2001; Bounoua et al. 2002; Zhao and Pitman 2002; Findell et al. 2007). The impact of perturbations to the land cover under enhanced greenhouse gas levels has also been examined (Costa and Foley 2000; Zhao et al. 2001; Bala et al. 2007).

There is no doubt that large-scale land cover change strongly affects the regional climate over the areas subject to land clearance. Model experiments conducted using global climate models and regional climate models confirm this (Chase et al. 1999; Wang et al. 2003; Hahmann and Dickinson 1997; Heck et al. 2001; Narisma and Pitman 2003). However, there is no agreement on the impact of LCC on climate in areas far from the perturbation, nor has an assessment of the impact of LCC relative to other more well-studied forcing terms been systematic. The examination of the regional significance of land cover change in comparison to increased greenhouse gases has been undertaken (Pitman and Zhao 2000; Bala et al. 2007; Betts 2001; Betts et al. 2004) but more work on this is needed. The issue of remote teleconnections—where LCC is in, for example, South America—is used to explain changes over another continent has been addressed many times. Some authors find clear teleconnections (e.g., Gedney and Valdes 2000; Werth and Avissar 2002, 2005), while others do not (Findell et al. 2007).

While large-scale land cover change can affect regional climate, it is useful to place the scale of this impact into some context. There are two important questions that remain outstanding. First, do SST anomalies resulting from natural variability [e.g., El Niño–Southern Oscillation (ENSO), North Atlantic Oscillation (NAO)] or anthropogenic factors (i.e., the twentieth-century warming trend) impact regional climates more or less than land cover change? Clearly, SST anomalies are generally remote from the continents where people live; hence the effect of SST anomalies on regional climate compared to LCC can provide a relative measure that prioritizes where effort might best be expended to improve regional simulations. Second, can LCC anomalies cause remote, nonlocal changes in climate? ENSO, for example, manifests as a well-known global forcing on climate. If land cover change can be shown to affect the global climate on a scale equivalent to ENSO or other major SSTs anomalies, then the omission of land cover change in global projections (e.g., those used in the fourth assessment report of the IPCC) would be very limiting.

The purpose of this study is, therefore, to compare the relative climatic impacts of these different forcing fields—SST anomalies and historical LCC—with experiments using the same general circulation model and the same experimental framework. This will help resolve open questions regarding the strength of the climatic response to LCC, although the inherently different time scales associated with the different forcing fields must be considered. The LCC scenario used in these experiments represents many centuries of anthropogenic alterations to the earth's surface, while an SST anomaly such as ENSO is a transient phenomenon. These issues will be discussed in more detail in section 5. First, the model and the experiments are briefly described in the next section. Globally averaged impacts are then considered, followed by a detailed consideration of the regional response to LCC and to imposed SST anomaly patterns. A discussion follows in section 5, and conclusions are given in section 6.

2. Model description and experimental design

The climate model is composed of an atmospheric general circulation model coupled to an ocean with

TABLE 1. Configuration of experiments discussed in this paper.

Experiment	SST field	Land cover field
Control	Climatology (1901–2004); Fig. 1a	Potential natural vegetation
LCC	Climatology (1901–2004); Fig. 1a	1990-like conditions
WTr	Climatology + global trend anomaly; Figs. 1a,b	Potential natural vegetation
WENSO	Climatology + tropical Pacific anomaly; Figs. 1a,c	Potential natural vegetation
WNAO	Climatology + North Atlantic anomaly; Figs. 1a,d	Potential natural vegetation

prescribed SST. The model grid cells are 2° latitude × 2.5° longitude, with 24 vertical levels in the atmosphere. The model has a seasonal and a diurnal cycle of insolation. The model's treatment of the atmosphere and land is the same as that in the Climate Model version 2.1 (CM2.1; Delworth et al. 2006). General characteristics of the land model are described below, since it is such a crucial factor in this series of experiments. Additional model documentation is available from the Geophysical Fluid Dynamics Laboratory (GFDL) Web site (online at http://nomads.gfdl.noaa.gov).

a. Land model description

The land model in CM2.1 was developed from the Land Dynamics (LaD) model described in Milly and Shmakin (2002, hereafter MS02). When the model was coupled to GFDL's atmospheric model, further tuning resulted in some parameter changes, described in GFDL Global Atmospheric Model Development Team (2004). Minor alterations to the land surface scheme were also made when the atmosphere–land model was coupled to the dynamic ocean model; these are described in Delworth et al. (2006).

The general characteristics of the land model at unglaciated points include three water reservoirs: snowpack, root-zone soil water, and groundwater. Evapotranspiration from soil is limited by a non-water-stressed bulk stomatal resistance and a soil-water-stress function, and drainage of soil water to groundwater occurs when the root-zone water capacity is exceeded. Discharge from groundwater to surface water is proportional to groundwater storage. Model parameters are temporally invariant but vary spatially as functions of vegetation and soil types.

The land model contains a series of vegetation-dependent parameters that characterize the land, including the maximum root-zone soil water (W_R), surface roughness length (z_o), non-water-stressed bulk stomatal resistance (r_s), snow-free surface albedo (A_n), snow-masking depth (W_S), and the effective rooting depth of the vegetation (Z_R). Values of z_o, r_s, A_n, and Z_R are determined from biome-based summaries and other field data, as described in MS02 and references therein. Here W_R is a product of the available water capacity of the soil type and Z_R. The derivation of Z_R detailed in MS02 is consistent for all vegetation types except desert and is dependent on biome-based surface-root-biome densities and root extinction depth scales. A critical value for root biomass in the function for the effective rooting depth is taken to be globally constant and is tuned in order to give typical forest rooting depths of about 1 m. Desert values of r_s and Z_R were arbitrarily set to 0 and 1: a guarantee that desert cells will retain nearly all precipitation and return it to the atmosphere. Further details of the land model are discussed in MS02.

b. Experimental design

There are three types of model simulations examined in this study: 1) an experiment forced by LCC; 2) experiments forced by patterns of interannual SST variability, though applied throughout the 60 yr of the experiments; and 3) an experiment forced by a long-term trend in SST, also applied uniformly throughout the 60 yr integration. This experimental design was formulated to assess the relative impacts of LCC against the impacts of well-known modes of natural SST variability and long-term change. The two modes of natural SST variability examined are those due to ENSO and the NAO. Details of how the associated SST anomaly forcing is formulated appear below. Table 1 lists the key land and sea surface forcing fields for the experiments discussed in this manuscript.

The control case for this series of simulations is a 60-yr integration with annually repeating climatological SSTs derived from the Hadley Centre monthly SST database (HadISST1; Rayner et al. 2003) for the years 1901–2004 (Fig. 1a). All simulations had concentrations of atmospheric greenhouse gases and other radiative forcing constituents fixed at 1990 levels (see Knutson et al. 2006 for details on the various forcings used in these simulations). The land cover field used in the control experiment was a potential natural land cover distribution: an approximate representation of the land cover conditions that would exist in the absence of human disturbance.

The land cover change experiment was a 60-year-long integration with the land cover field fixed at 1990-like conditions. The land cover perturbation did not include

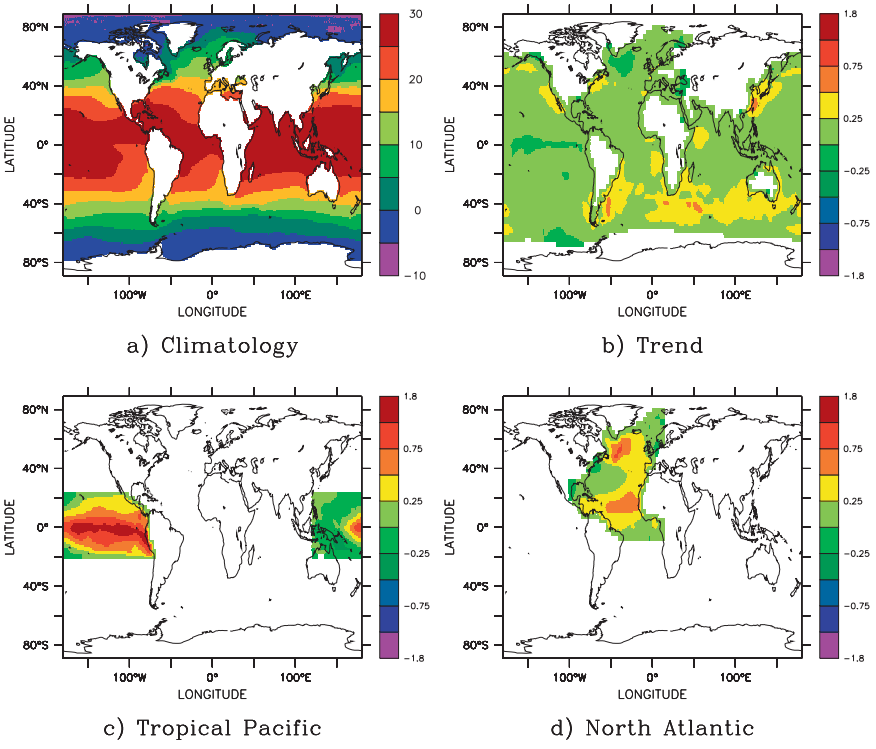

FIG. 1. SST forcing patterns (°C) (a) climatology derived from the Hadley Centre dataset spanning the years 1901–2004; (b) warming trend anomaly; (c) tropical Pacific ENSO-like warm-phase anomaly; and (d) North Atlantic NAO-like warm-phase anomaly.

the release of greenhouse gases that would accompany deforestation or the uptake of carbon dioxide that would result from reforestation. The experiments with altered SST had a spatially varying anomaly pattern added to the climatological field used in the control run, as discussed in the next section. These runs were also integrated for 60 yr. All other settings in these simulations were identical to those in the control run. Analyses were performed on the final 50 yr of each model run. Details of the SST anomalies and the land cover distributions are discussed below.

c. *SST forcing fields*

Figure 1a shows the SST climatology derived from the Hadley Centre data spanning the years 1901–2004 (Rayner et al. 2003). A rotated empirical orthogonal function (EOF) analysis (Kaiser 1958) identified the three leading patterns of interannual SST variability as the linear trend of global SST, a warm-phase ENSO-like pattern, and a warm-phase NAO-like pattern. These patterns represent 27.2%, 20.5%, and 5.8% of the global SST variance. Although the third EOF explains such a small percent of the global variance, it does explain up to 70% of the local variance in the region of the intertropical convergence zone (ITCZ) during northern summer. To avoid ice contamination, we restricted the analysis to ice-free points.

These patterns are scaled by the standard deviations of the principal components to create physical values. The warm-phase ENSO and warm-phase NAO patterns (hereafter referred to as WENSO and WNAO) are multiplied by twice the standard deviation of their respective principal components to create patterns similar to those observed in strong ENSO and NAO years (Figs. 1c,d), while the linear warming trend (WTr) is multiplied by one standard deviation to maintain a pattern with historical relevance (as opposed to a future warming pattern; Fig. 1b). To focus the anomaly on the center of the ENSO region, only the tropical portion of the second EOF is used (Fig. 1c). These anomalies are then added to the climatological seasonal cycle of SST and used as the new boundary condition of the model's simulation.

In none of the experiments do we permit the SST- or LCC-forced response in the atmosphere to feedback and alter SST. Thus, while our experiments provide clear insight into the way SST anomalies and LCC can alter regional climate properties, they overlook the interesting question of further feedbacks and coupling to the SST fields. Such a study would require a full dynamic

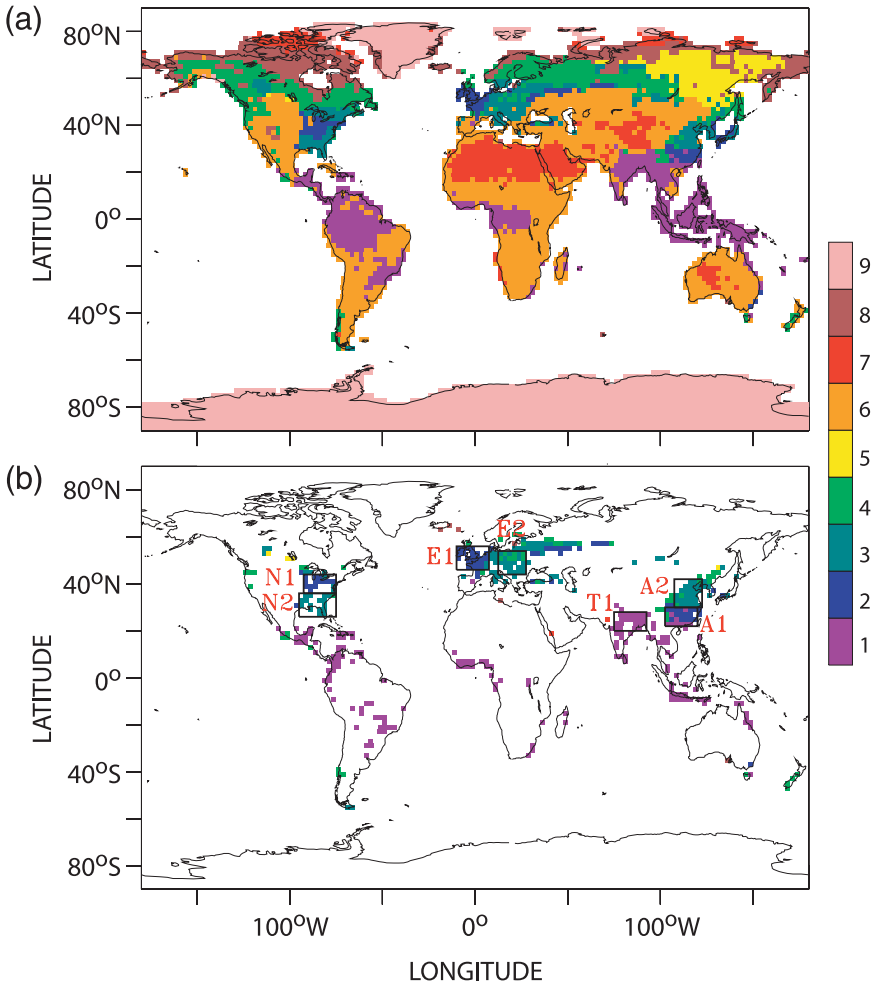

FIG. 2. (a) Preanthropogenic cover type distributions. 1 = broadleaf evergreen, 2 = broadleaf deciduous, 3 = broadleaf/needleleaf, 4 = needleleaf evergreen, 5 = needleleaf deciduous, 6 = grassland–crops–pasture, 7 = desert, 8 = tundra, 9 = glacier. (b) Differences in cover type between the 1990 distribution and the preanthropogenic distribution; 11.6% of the land surface is converted to grasslands. Colors in (b) are representative of the original cover type shown in (a). Boxes in (b) are used to indicate regions used in analyses and discussion later in the paper: North American boxes: N1, N2; European boxes: E1, E2; Asian boxes: A1, A2; tropical box: T1.

coupled model with an interactive ocean, which is beyond the scope of the present study

d. Land cover reconstructions

The potential natural land cover distribution (Fig. 2a) approximates the land cover conditions that would exist in the absence of human disturbance. It is based on the MS02 classification used in the LaD. LaD has 10 vegetation types that are groupings of the 32 Matthews vegetation types (Matthews 1983). The LaD vegetation types include broadleaf evergreen, broadleaf deciduous, mixed forest, needleleaf deciduous, needleleaf evergreen, grassland, desert, tundra, and ice. Parameter values for each of these cover types are listed in Table 2. MS02 include an agriculture type in the LaD code, but parameter values for this type are highly uncertain and have not been tested. We therefore use the grassland type to represent crops and/or pastures, an approximation used in other studies as well (e.g., Hansen et al. 1998; Matthews et al. 2003). Some observational studies also provide support for this assumption. Mahmood and Hubbard (2002), for example, show that nonirrigated crops and natural grasslands in Nebraska (central United States) produce similar fluxes of heat and moisture. Twine et al. (2004), on the other hand, show that crops and grasslands do produce different climatic signals.

TABLE 2. Minimum bulk non-water-stressed (NWS) stomatal resistance, effective rooting depth, snow-free albedo , roughness lengths, and the critical snowmass (the snow amount that covers half of the surface) used in momentum and surface flux calculations for land cover types used in the GFDL land surface model.

	NWS stomatal resistance (s m^{-1})	Effective rooting depth (m)	Snow-free albedo (−)	Roughness length (m)	Critical snowmass (kg m^{-3})
1 broadleaf evergreen trees (BE)	43.6	1.30	0.149	2.65	60
2 broadleaf deciduous trees (BD)	131.0	1.38	0.130	0.90	10
3 broadleaf/needleleaf trees (BN)	87.1	1.61	0.132	1.20	25
4 needleleaf evergreen trees (NE)	69.7	0.84	0.126	0.90	40
5 needleleaf deciduous trees (ND)	218.0	0.84	0.143	0.80	40
6 grassland (G)	56.6	0.98	0.182	0.07	5
7 desert (D)	0.0	1.00	0.333	0.01	5
8 tundra (T)	170.0	0.49	0.139	0.07	5

However, Gibbard et al. (2005) suggest "that to estimate the potential range of response to land cover change in a coupled model, it would suffice to consider only two types of vegetation: forest vs. grass and shrublands."

LaD prescribes a single dominant vegetation type for each grid cell and, therefore, does not represent subgrid-scale heterogeneity. It is difficult to assess the impact of this limitation. Some previous research indicates that the heterogeneous nature of much real-world deforestation may induce mesoscale circulation changes (e.g., Avissar and Pielke 1989; Burke et al. 2000). Future model developments will enable us to include subgrid-scale heterogeneity and better address this question.

The 1990 land cover type distribution was derived by combining the potential vegetation distribution described above with the reconstruction of global land use history detailed by Hurtt et al. (2006). Figure 2b shows the differences between the natural and 1990 cover type maps; 11.6% of the earth's land surface differs (was converted from native forests to grassland) between the two cover type distributions. Additionally, according to the Hurtt et al. (2006) database, transitions from natural grasslands to crops or pastures occurred on about 15% of the land, but these transitions do not appear in Fig. 2 because of our treatment of grassland, crops, and pastures as one cover type. This estimate of land area converted from a potential, undisturbed state to crops or pastures is within the range of similar estimates provided by other studies (Vitousek et al. 1997; Ramankutty and Foley 1999; Chase et al. 2000; Pitman and Zhao 2000; Klein Goldewijk 2001).

The conversion of the potential natural vegetation to grasslands that is depicted in the change from the control simulation to the LCC simulation includes changes in parameters controlling the use of available water and energy at the surface. In the LaD scheme, altered surface parameters include the rooting depth, non-water-stressed bulk stomatal resistance, surface roughness length, snow-free surface albedo, and snow-masking depth. These alterations are discussed in detail in Findell et al. (2007), with a full framework describing the physical pathways of change resulting from these parameter changes. The LCC scenario used in this study is the same as the one in Findell et al. (2007). Their Fig. 3 and the parameter values given in Table 2 show that the conversion of forests to grasslands leads to smaller root-zone water capacity, higher surface albedo, and shorter roughness lengths in each of the regional boxes in Fig. 2b. The stomatal resistance is reduced in all the nontropical boxes in Fig. 2b and increased in the areas that are converted from broadleaf evergreen trees to grasslands (all of T1 and some grid cells in A1). Findell et al. (2007) show that these competing influences result in statistically significant reductions in evapotranspiration and net radiation in each of the regional boxes shown in Fig. 2b. That conclusion is supported in Fig. 3 of this paper, which shows significant reductions in annual global mean evaporation and net radiation as a result of the prescribed LCC. Figure 3 also shows that there is effectively no change to the global mean shortwave radiation, implying that any decrease in shortwave radiation resulting from the increased albedo that accompanies LCC is balanced by an increase in shortwave radiation resulting from decreased low cloud cover, which follows from increased sensible heat flux and surface temperature, as described in Findell et al. (2007).

e. Statistical methods

The modified Student's *t* test of Zwiers and von Storch (1995) and von Storch and Zwiers (1999) is used to compare differences between the 50-yr time series of each variable produced at each model grid cell. This test is more rigorous than the standard *t* test because it accounts for autocorrelation within the time series, therefore reducing the rate of false positives (false determinations of a climate signal resulting from the given perturbation).

Neither the standard nor the modified *t* test accounts for spatial correlation within fields (Von Storch and

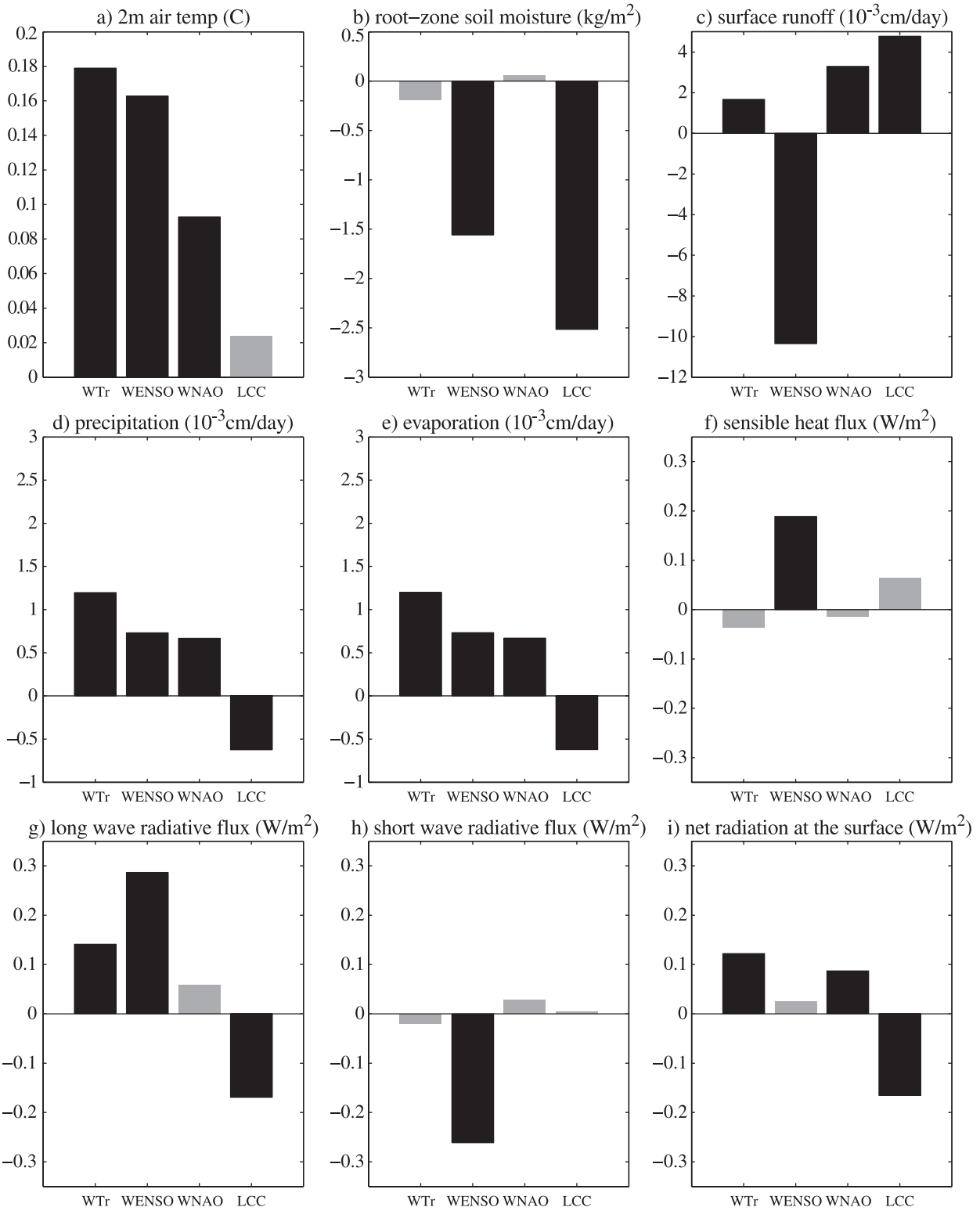

FIG. 3. Annual global mean differences between the four experiments and the control (labels as in Table 2). Black (gray) bars indicate significance (nonsignificance) at the 95% level according to the modified *t* test.

Zwiers 1999). Variables such as 500-mb geopotential height have large correlation length scales, meaning that data from adjacent model grid points are not independent, and the effective number of spatial degrees of freedom (dof) is much smaller than the number of grid points. Because of this interdependence between grid points, more than 5% of the area of interest must pass the 95% significance test for the field result as a whole to be statistically significant. Livezey and Chen (1983) present a methodology for determining field significance through an application of the binomial theorem. In their Fig. 3, they show the relation between the estimated percent of local (e.g., at a model grid point) 95% significance tests passed that will be equaled or exceeded by chance 5% of the time versus the number of spatial dof. This plot shows that, for a field with 40 dof, 12.5% of the field must pass local 95% significance tests for the result as a whole to be statistically significant at the 95% level. Similarly, a field with 20 dof requires about 15% of the field to pass the individual 95% significance tests, 100 dof requires about 9.5%, 200 dof requires about 8%, and 1000 dof requires about 6%.

To apply the Livezey and Chen (1983) results to the annual mean global results of this study, estimates of the effective degrees of freedom are needed for each variable. A full Monte Carlo simulation would be required to obtain these values directly; instead, we used published estimates for approximate degrees of freedom suitable for this study. These published estimates of global degrees of freedom values (see, e.g., Van den Dool and Chervin 1986; Wang and Shen 1999) range from the high twenties to a few hundreds, depending on variable, season, and spatial and temporal scales. Though these studies do not provide independent degrees of freedom estimates for all variables, they do give approximate bounds on the degrees of freedom for many fields. We will use a conservative value of 40 degrees of freedom to guide interpretation of the results presented in the following sections. As mentioned above, a field with 40 dof requires 12.5% of grid cells to pass local 95% significance tests for the field to be significant at the 95% level.

3. Global-scale impacts

Table 3 shows, for each of the four experiments, the percent of global area and land area with significantly different annual mean 2-m air temperature from the control simulation. Precipitation, evaporation, sensible heat flux, root-zone soil moisture, and runoff are also included. Additionally, Fig. 3 shows the magnitude of the globally averaged annual mean differences from the control experiment for nine variables for each of the four perturbation experiments, while Figs. 4 and 5 show global maps of the annual mean differences for 2-m air temperature and precipitation, respectively.

TABLE 3. Annual mean differences between the control run and each of the four experiments, in the percent area (full globe or just land) that passes a 95%-level modified t test. T_ref = 2-m air temperature; P = precipitation; E = evaporation; H = sensible heat flux; SM = root-zone soil moisture; Q = surface runoff. Values greater than 12.5% are shown in bold to indicate increased likelihood of field significance (see discussion in section 2c).

	Ocean + land				Land only					
	T_ref	P	E	H	T_ref	P	E	H	SM	Q
WTr	**72**	**14**	**27**	**21**	**43**	9	11	8	8	7
WENSO	**60**	**52**	**58**	**54**	**55**	**43**	**45**	**45**	**39**	**29**
WNAO	**37**	**19**	**27**	**24**	**41**	**16**	**16**	**17**	**14**	**13**
LCC	8	5	10	8	**13**	8	**14**	11	**14**	12

The near-global SST forcing in the WTr experiment produces a global surface air temperature response that passes the 95%-level modified t test in 72% of the globe and over 43% of land area (Table 3; Fig. 4a). The average surface air temperature is 0.18°C warmer in the WTr experiment than in the control run (Fig. 3a). Globally averaged precipitation and evaporation both increase by about 0.0012 cm day^{-1} (Figs. 3d,e), while the sensible heat flux decreases by a statistically insignificant amount (about 0.04 W m^{-2}; Fig. 3f). Though the global average precipitation change is statistically significant, only 14% of the total area and 9% of the land area have significantly different annual precipitation, and the magnitude of the change is nowhere greater than 0.1 cm day^{-1} (Fig. 5a). Evaporation and sensible heat flux are altered over about a quarter of the globe (27% and 21%, respectively), but the impact only reaches about 10% of land area. The strong temperature response to the WTr perturbation (affecting 43% of land area) compared to the weaker response in precipitation (9%) is an indication of why it is more difficult to detect changes in rainfall and attribute them to global warming (e.g., Zhang et al. 2007).

The WENSO SST forcing also has broad, global impacts, with 60% of global area and 55% of land area experiencing significantly different temperatures than the control simulation. Unlike the WTr experiment, the surface temperature impact is not just a warming signal: much of the United States, Mexico, eastern Russia, and northern China are significantly cooler (by more than 1°C; Fig. 4b). Larger areas, however, do show warming in excess of 1°C (e.g., northern North America and northern South America, Australia, India, and eastern Africa; Fig. 4b). The global average annual mean temperature is 0.16°C warmer than the control simulation (Fig. 3a). This value gives an indication of the impact

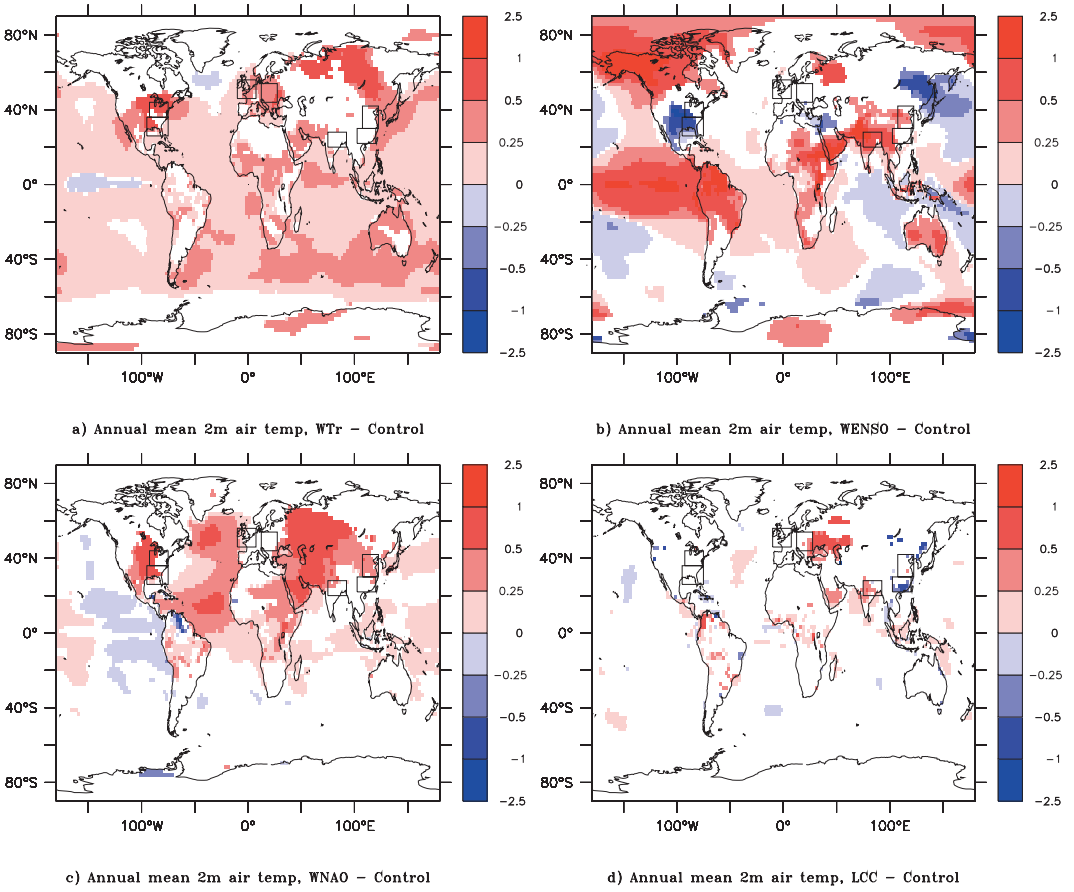

FIG. 4. Annual 2-m reference air temperature differences (°C) between the four experiments and the control simulation. (a) WTr − control; (b) WENSO − control; (c) WNAO − control; (d) LCC − control. Differences are only shown where they are statistically significant at the 95% significance level according to the modified *t* test.

that an El Niño event has on the often-cited metric of global mean air temperature, for example, the high temperatures noted in the long-term record in 1998 (see, e.g., Thompson et al. 2008). The WENSO forcing produces an impact on other variables that is significant over more than half the globe (Table 3) and leads to significant globally averaged differences in eight of the nine variables shown in Fig. 3 (all but net radiation at the surface). Even over land, where the SST forcing is obviously not local, 39%–45% of the area has significantly different precipitation, evaporation, sensible heat flux, and soil moisture (Table 3). In general, the nonsignificant land areas for these four variables are north of 50°N in North America and north of 40°N in Asia (precipitation shown in Fig. 4b). A strong precipitation response is obvious in the Indian and Pacific Oceans.

The WNAO forcing is associated with warming in excess of 0.5°C over the region of the SST anomaly, much of western Asia through the Middle East, and throughout central North America (Fig. 4c). Modest warming is also seen over much of South America and Africa. In total, 37% of global area and 41% of land area have a significantly different 2-m air temperature from the control simulation, with a statistically significant globally averaged annual mean increase of 0.09°C (Fig. 3a). The areas of significant differences are smaller for other variables: 19%–27% for global precipitation, evaporation, and sensible heat flux, and 13%–17% for land-only values of those three variables, soil moisture, and runoff (Table 3). Surprisingly, the magnitude of the globally averaged annual mean increase in both precipitation and evaporation is equivalent to that of the WENSO experiment (about 0.0007 cm day^{-1}; Fig. 3), and the mean global temperature increase of 0.09°C is more than half the 0.16°C of the WENSO experiment.

In contrast to the broad impact of each of the SST anomalies, the LCC experiment produces statistically significant surface air temperature changes over only 8% of global area and 13% of land area. The globally averaged temperature difference of 0.023°C is not

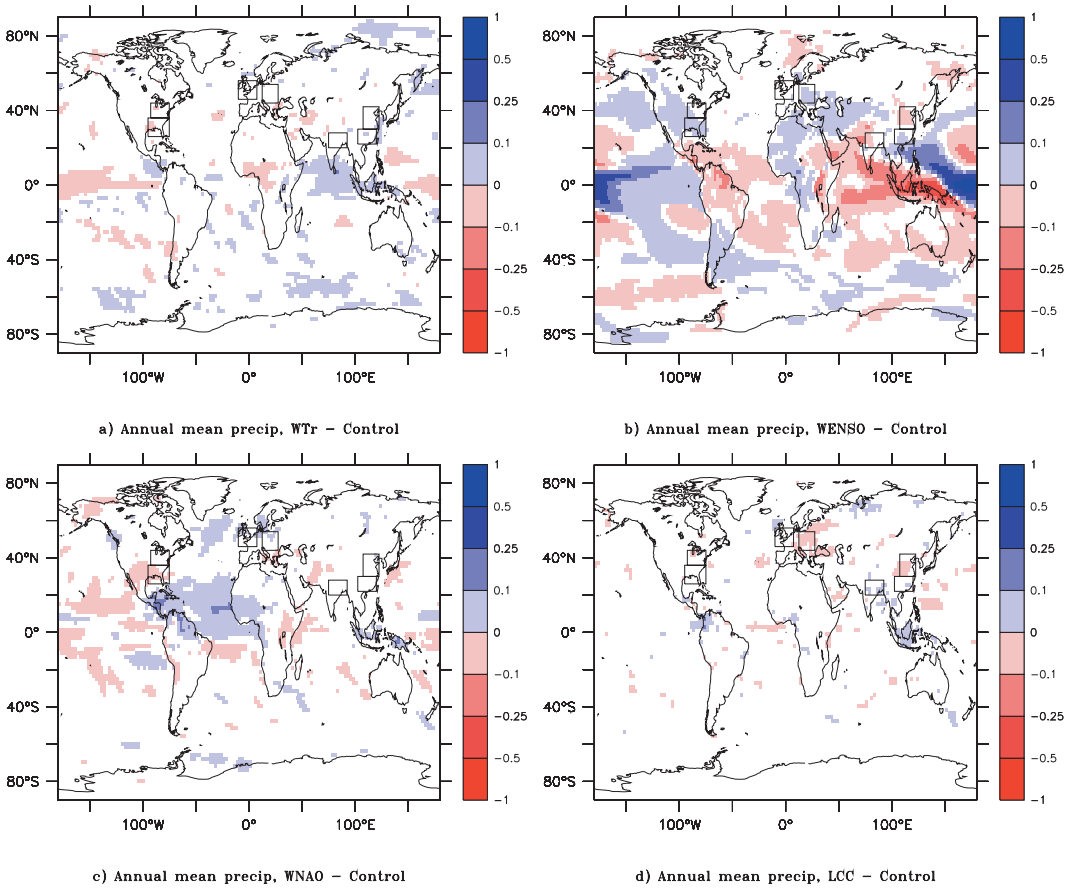

FIG. 5. As in Fig. 4, but for annual precipitation differences (cm day^{-1}).

statistically significant at the 95% level (Fig. 3a). For the other variables listed in Table 3, only between 5% and 10% of global area shows a significant difference from the control simulation. Given the discussion of field significance in section 2c, it is unlikely that the global impact of the LCC experiment would pass field significance requirements. The land-only values in Table 3 show that 8%–14% of land area is significantly different from the control run. Two-meter air temperature, evaporation, and root-zone soil moisture all exceed the 12.5% threshold needed for a field with 40 dof to be statistically significant at the 95% level. Nevertheless, this 8%–14% of land area passing the significance test should be considered alongside the fact that 11.6% of the land surface has altered vegetation in the LCC experiment. Given the bulk of previous research indicating that this sort of LCC should induce a local response (Betts et al. 1996; Pitman 2003), the 8%–14% range might simply indicate the direct response to LCC and does not necessarily imply the existence of teleconnections beyond the altered regions. However, the globally averaged values of soil moisture, surface runoff, precipitation, evaporation, longwave heat flux, and net radiation at the surface are each significantly different from the control run values at the 95% confidence level, suggesting that, in the areas where changes occur, their magnitudes are relatively large and consistent in sign (Fig. 3).

Thus, in broad terms, Table 3 shows that the WTr, the WENSO, and the WNAO SST forcings drive a large-scale response in temperature. The scales of the changes in temperature globally and over land are large, exceeding 40% of land area at a 95% significance level. In contrast, the land cover change anomaly causes a much smaller impact at the scale of the continents. The WENSO forcing dominates the precipitation impact over land in terms of spatial extent, though all forcings lead to statistically significant changes in the global average annual mean precipitation rate (Fig. 3). When we focus on terrestrial quantities such as evaporation, sensible heat, soil moisture, and runoff, while the WENSO pattern remains the forcing with the broadest impact, LCC is at least equivalent to the WTr and WNAO forcings over land.

While the *continental*-scale impacts of LCC are relatively small, though statistically significant in some cases, the impacts of LCC are much broader when analyzed regionally. The LCC perturbation is likely to be most important over the regions where the perturbation is imposed. We therefore assess the impact of LCC over those regions shown in Fig. 2 relative to the regional impact of the SST anomalies. Given that the imposed SST anomalies are commonly understood to have important impacts on regional climate, identifying the impact of LCC relative to these SST anomalies over the regions of LCC provides a clear demonstration of the significance of LCC to regional climate. However, regions of LCC may not necessarily coincide with regions of extensive natural variability associated with the SST patterns considered here, so this selection of regions may bias the results toward LCC significance. In particular, Figs. 4 and 5 show that precipitation and temperature in northern South America and the islands of Oceania are sensitive to the imposed SST anomalies. These regions are not considered here because of a lack of large-scale LCC in the depiction shown in Fig. 2. Furthermore, Figs. 4 and 5 also show that LCC does lead to some significant differences in areas without LCC, most notably the broad area of warming north of the Black and Caspian Seas (Fig. 4d). Given that there is no statistically significant accompanying change in precipitation (Fig. 5d), evaporation, sensible heat flux, soil moisture, or runoff (not shown), it is likely that the surface temperature signal results from being in the predominately downwind direction from European regions with substantial LCC.

4. Regional-scale impacts

Figures 6–10 show regionally averaged seasonal cycles of seven variables (2-m air temperature, root-zone soil moisture, precipitation, evaporation, sensible heat flux, net radiation at the surface, and surface runoff) for five areas with substantial land cover conversion (see boxes in Fig. 2b). In addition to the seasonal cycles for each of the five model simulations, monthly differences from the control run are displayed, along with the number of months that each experiment is significantly different from the control, according to the 95%-level modified t test. Conservatively, we might expect one month per year to pass this significance test by chance for each experiment. We now discuss each of these five regions in detail.

a. European regions

For the eastern European region (E2 in Fig. 2b), Fig. 6 shows that the LCC and WENSO experiments are both important in determining the seasonal cycle of components in the water and energy cycles, while the WTr and WNAO experiments do little to alter the climatology determined by the control simulation. The weak response over region E2 from the WNAO forcing agrees with similar simulations by Magnusdottir et al. (2004). Using much stronger SST forcing than in our WNAO experiment, Magnusdottir et al. (2004) find the most substantial precipitation anomalies occur over the North Atlantic Ocean, with little propagation eastward over continental Europe.

In the LCC simulation, the vegetation in this eastern European region (E2) is converted from a mixture of broadleaf and needleleaf trees to grasslands. This land cover conversion is characterized by a substantial reduction in the effective rooting depth of the vegetation, which is accompanied by significantly less root-zone soil moisture and evaporation through the year, an increase in sensible heat flux (significant April through December), and decreased net radiation (significant in seven months of the year). The increase in sensible heat flux is maximized in July, at which point the 2-m air temperature is also significantly warmer than the control simulation by about 1°C. Precipitation is slightly reduced throughout the year, though the difference is only significant in April, July, and August.

The WENSO SST anomaly drives a response in region E2 of similar magnitude but opposite sign from LCC. Soil moisture is significantly increased from July through February, forced by an increase in summer precipitation (significant in July and August) and a decrease in sensible heat flux (significant July through September). There is also increased evaporation (significant August through October) and increased runoff (significant July through February) in response to this SST forcing. Net radiation is not significantly changed. Surface temperature is significantly cooler in August by almost 1.5°C and significantly warmer in March by about 0.8°C. These changes in precipitation and seasonal air temperature anomalies over eastern Europe agree with other ENSO SST-forced model simulations (e.g., Deser et al. 2006).

We do not show results from western Europe (region E1). While LCC had a large impact on soil moisture, as expected with the conversion from broadleaf deciduous trees to grasslands, and a significant impact on spring and summer evaporation and winter and spring runoff, there was no impact on rainfall or temperature. The seasonal response in region E1 to each of the experiments is similar to the response in region E2, but with reduced magnitude and significance. This region appears to be relatively insensitive to any of the imposed anomalies.

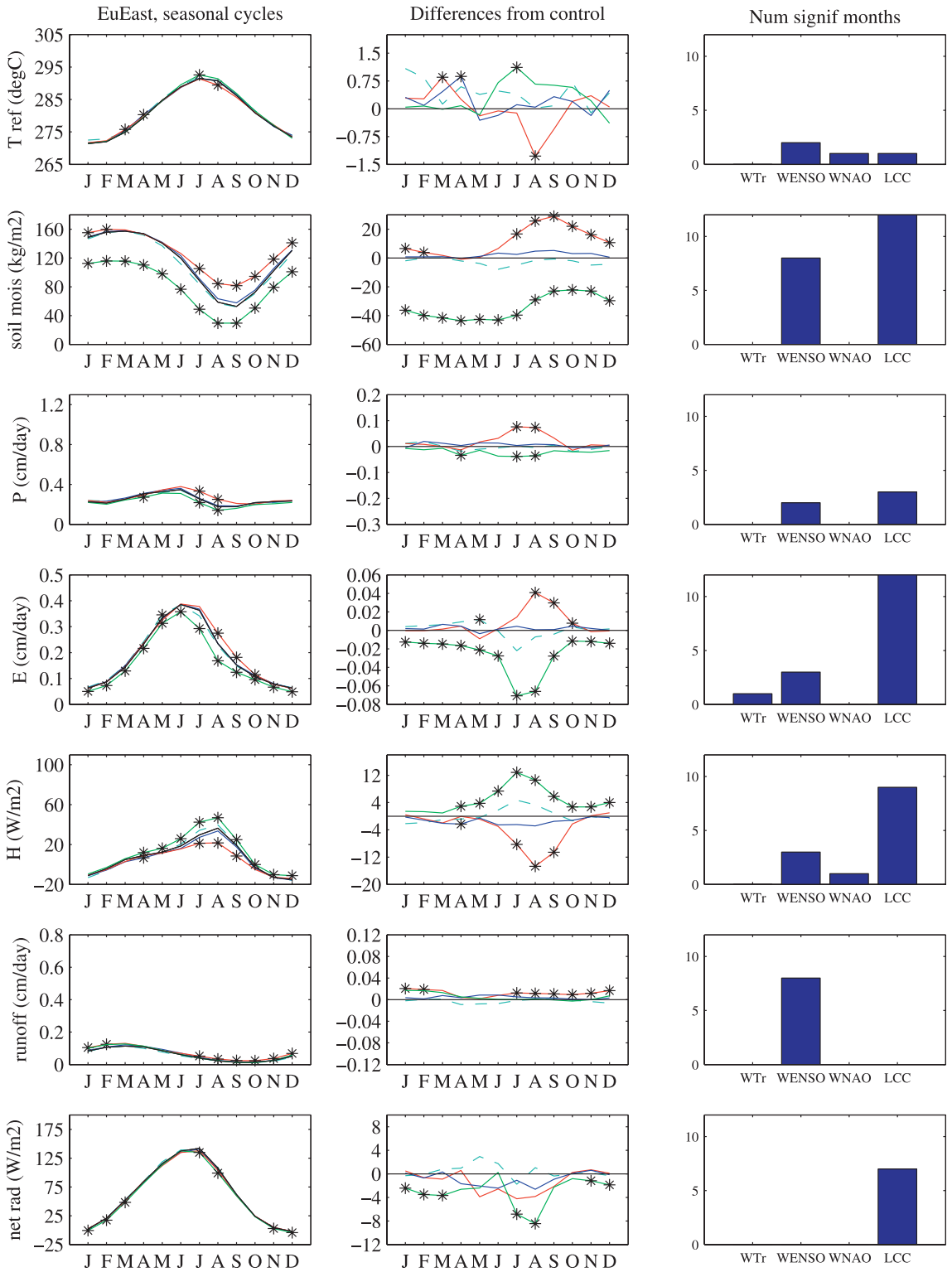

FIG. 6. (left) Regional averages in the eastern European box (E2 in Fig. 2) of seasonal cycles of 2-m air temperature (T_ref), soil moisture, sensible heat flux H, precipitation P, evaporation E, and surface runoff for the control run (black line); WTr (cyan, dashed), WENSO (red), WNAO (blue), and LCC (green). Black asterisks indicate significance at the 95% level according to the modified t test for that month. (middle) Differences from the control run. (right) Number of significant months for each of the four perturbation experiments.

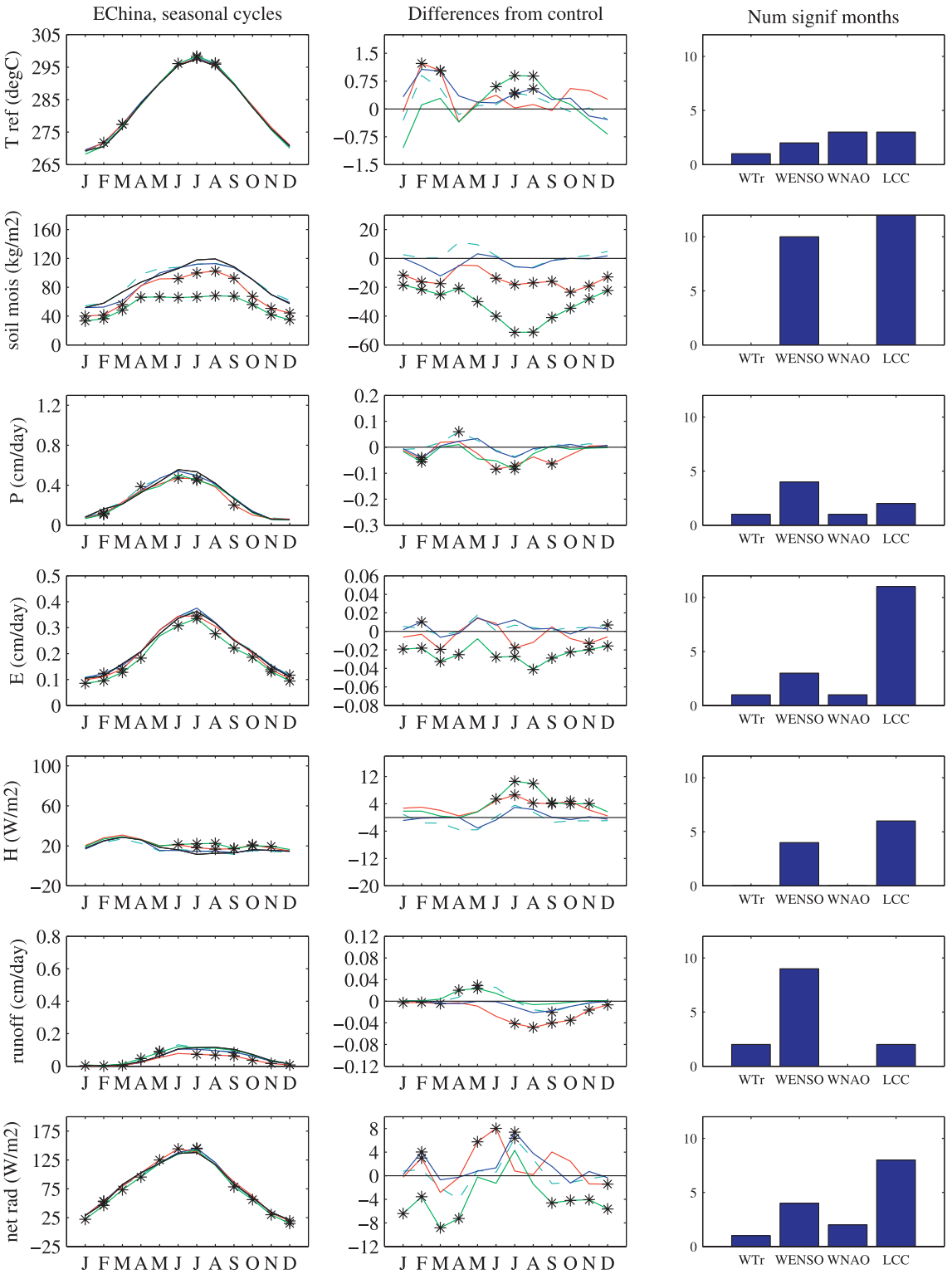

FIG. 7. As in Fig. 6, but for region A2.

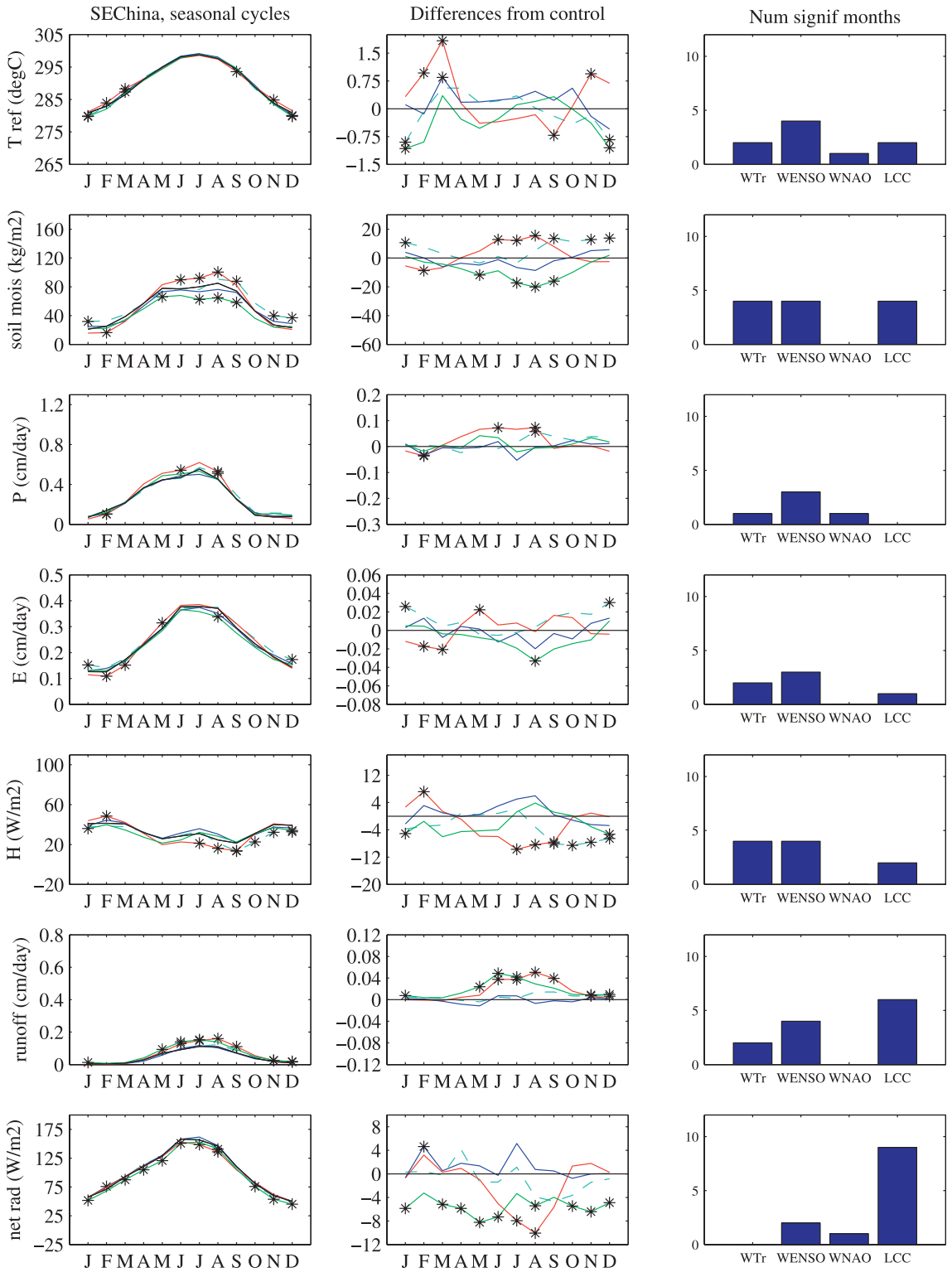

FIG. 8. As in Fig. 6, but for region A1.

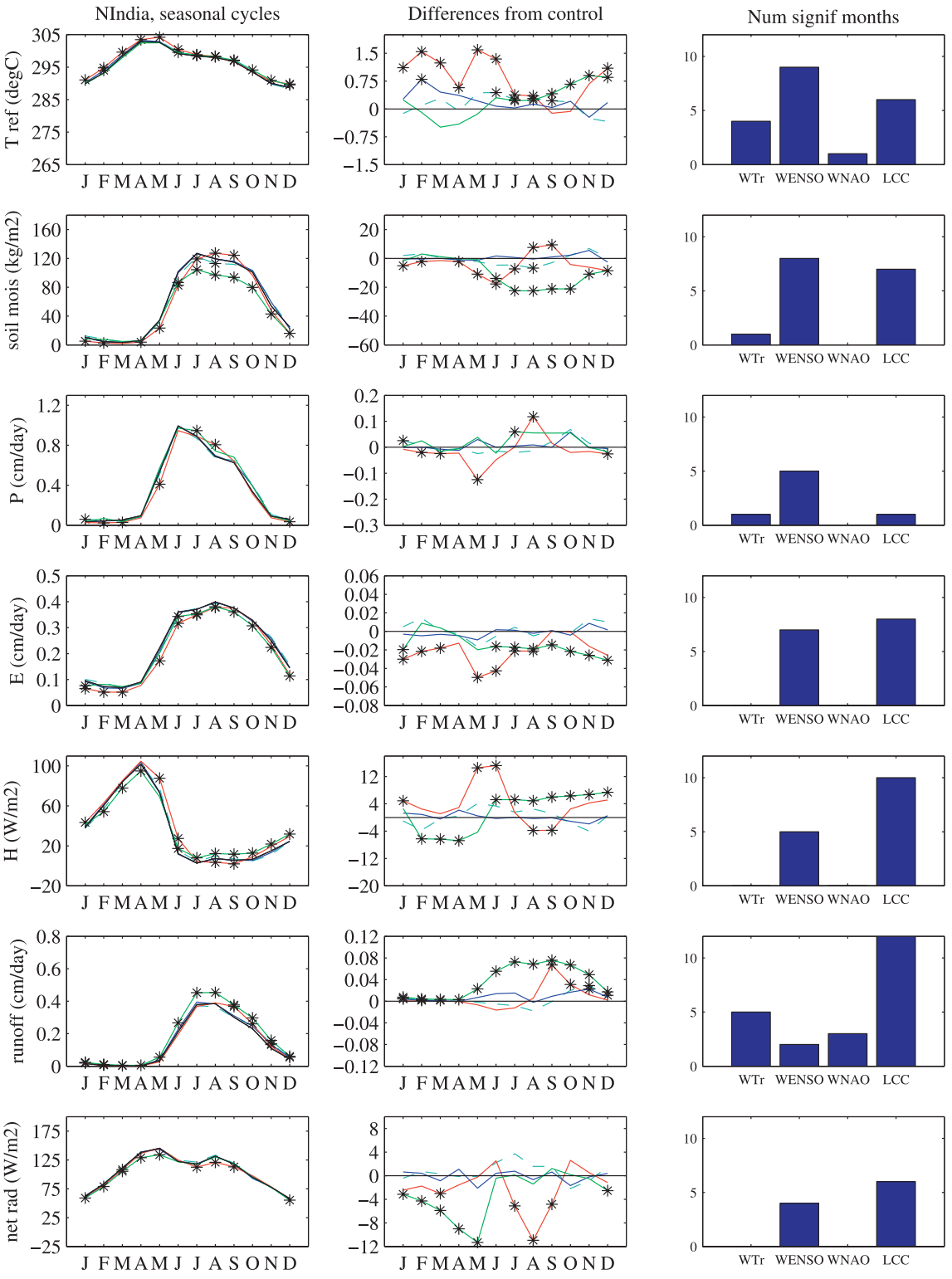

FIG. 9. As in Fig. 6, but for region T1.

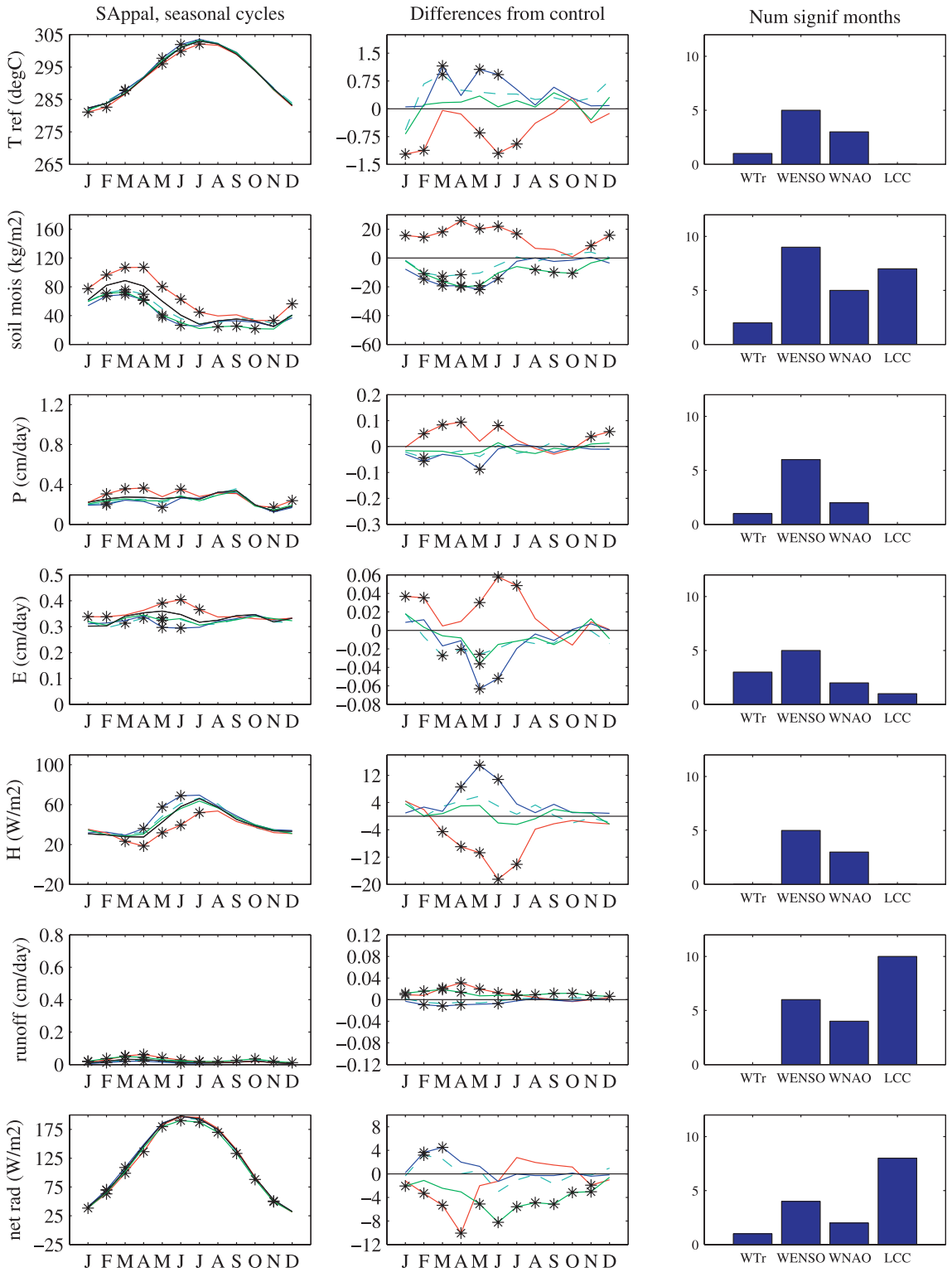

FIG. 10. As in Fig. 6, but for region N2.

b. Asian regions: Region A2

Figure 7 shows a large statistically significant reduction of soil moisture in region A2 in eastern China resulting from both LCC and WENSO. The change in soil moisture associated with LCC, which is significant every month of the year, is principally the result of the parameter changes accompanying the conversion from broadleaf and needleleaf trees to grasslands (e.g., reduction in effective rooting depth). The soil moisture change is accompanied by a decrease in evaporation (significant in every month except May), an increase in sensible heat flux during the warm months (significant June through November), and a reduction in net radiation from September. The large decrease in evaporation and increase in sensible heat fluxes associated with LCC affect temperature but only during the summer months. Precipitation is only significantly affected in February and July (reduced in both months). Runoff is significantly increased in April and May.

While the drying associated with LCC results from the prescribed changes to vegetation properties, the drying of soils in eastern China resulting from the WENSO forcing clearly must be driven by SST-induced changes to atmospheric fields. Precipitation is indeed significantly reduced in June, July, September, and February and evaporation is significantly reduced in March, July, and November. Sensible heat flux is significantly increased from June through November, but surface temperature is only significantly increased in February and March. Runoff is decreased from July through March. The signal of reduced rainfall over the A2 Asian region agrees with observed ENSO-phase precipitation anomalies (e.g., Dai and Wigley 2000).

Overall, the WENSO and the LCC experiments dominate the changes in this region. The WNAO experiment is significantly warmer in March, July, and August, but other fields are rarely significant. The WTr has no more than one significant month for each field in Fig. 7. The role of LCC in this region is clearly sufficient to require its inclusion in simulations that explore regional climate change.

c. Asian regions: Region A1

Figure 8 shows that the WTr, WENSO, and LCC experiments have roughly the same number of total significant months in region A1 in southeastern China, while the WNAO experiment has almost no significant impact. The impact of LCC is mainly restricted to a decrease in soil moisture (significant in four warm-season months), an increase in runoff (significant in six months of the year), and a decrease in net radiation (significant in nine months of the year).

In general, the WENSO experiment results in wetter and cooler summers and warmer and drier winters compared to the control simulation in region A1 (in agreement with the CCSM simulations of Deser et al. 2006), with significant changes to each of the fields shown in Fig. 8 in three or four months of the year. The WTr experiment forces significant changes in up to four months in each of the fields in Fig. 8, primarily during wetter and cooler winters.

The differences in response of regions A1 (to the south) and A2 (to the north) to the WENSO, WTr, and LCC anomalies highlight how two regions close together can be affected in quite different ways by different forcings. Both regions are in southeastern China, but the sign of the changes induced by the WENSO anomaly are reversed in the two regions during boreal summer (warmer and drier than the control simulation in A2; cooler and wetter in A1), WTr has almost no impact on A2, but does influence wintertime conditions in A1 to the south, and region A1 is substantially less affected by LCC than region A2.

d. Tropical region: T1

Figure 9 identifies the WENSO and LCC experiments as having the most significant climatic impacts in northern India (region T1). The WENSO experiment leads to significant warming and drying over northern India during the dry season and the transitional months (December through June; also seen in Deser et al. 2006). The LCC scenario (a conversion of tropical broadleaf evergreen trees to grasslands), in contrast, has little effect on rainfall, but leads to warming in July through December. Thus, the WENSO perturbation warms the region in the first half of the year while LCC warms it in the second half of the year. The WENSO experiment reduces evaporation in the first half of the year, while LCC decreases evaporation in the second half. LCC also substantially increases runoff and sensible heat flux and decreases evaporation through the second half of the year.

The WTr experiment increases temperature significantly for four months of the year during the rainy season but otherwise has a minor impact compared to LCC or WENSO, the only other notable signal being a significant increase in runoff during the dry season. The WNAO experiment has little significant impact over this region.

e. North American regions

The two Appalachian regions (N1 and N2 in Fig. 2b) respond in different ways to the various forcings, with more significant differences notable in the southern region (N2). Figure 10 shows the nearly equal-but-opposite impacts of the WENSO and WNAO experiments

on most fields in the southern Appalachians. The WNAO anomaly leads to drier and warmer conditions, while the WENSO anomaly leads to wetter and cooler conditions. This response to the warm-phase ENSO-like SST forcing is similar to that obtained by Deser et al. (2006). The WENSO impact is stronger than the WNAO, with between four and nine significant months (generally spring and summer) for each variable in Fig. 9. The WNAO signal is also felt most strongly during spring and summer, but only 2–5 months are significant for the variables in Fig. 10. The impact of the WTr experiment is similar in sign and seasonality to the impact of WNAO, though there are generally even fewer months with significant differences from the control.

In terms of the terrestrial variables, LCC is the dominant influence on runoff and net radiation in region N2, where the land cover was converted from broadleaf and needleleaf forests to grasslands, and is on par with the WENSO experiment in terms of soil moisture. These changes do not translate into significant changes in the turbulent energy fluxes, precipitation, or 2-m air temperature. Over the northern region, N1, all the forcings tend to have a substantially smaller impact. Thus, we find no evidence that LCC is an important driver of the atmospheric climatology in the Appalachian regions. Indeed, remote SST anomalies are more influential. However, if quantities like soil moisture and runoff are being used from the climate models, LCC is as significant a driver of the regional terrestrial quantities as the SST anomalies.

5. Discussion

At the global scale, our results show significant changes in air temperature, rainfall, evaporation, and surface runoff induced by each of the SST anomalies. Over land only, the WENSO and WNAO experiments dominate the perturbation to the precipitation and temperature fields with at least 2 and 3 times the land area, respectively, affected by each SST anomaly in comparison to LCC (Table 3). Thus, the land-only impact from LCC on temperature and precipitation covers a small area relative to the SST anomalies and is at the margin of statistical field significance. However, if changes in surface quantities (evaporation, sensible heat flux, soil moisture, runoff) are assessed, LCC impacts about as much area as the WNAO and WTr perturbations (Table 3), and the magnitude of these impacts is large enough to lead to statistically significant differences in the annual global mean values of soil moisture, surface runoff, precipitation, and evaporation (Fig. 3).

Despite these relatively large magnitude changes in regions of LCC, the results presented here show that changes to terrestrial quantities such as soil moisture and sensible and latent heat fluxes that result from LCC rarely propagate into the atmosphere in a significant way. Figure 11 shows a clear example of how dramatically the atmosphere over the Indian Ocean and Southeast Asia is altered by the WENSO experiment (Fig. 11b). The other forcing scenarios do not significantly alter the 850-mb wind or specific humidity fields (Figs. 11a,c,d), despite the substantial impact of LCC on evaporation, sensible heat flux, soil moisture, runoff, and even surface temperature in regions A1, A2, and T1 (Figs. 7–9). Figures 7–9 show that LCC and WENSO are essentially equally important at the terrestrial surface in these three regions, but Fig. 11 shows that while a broad atmospheric response is present in the ENSO-like experiment, the LCC impacts do not propagate beyond the surface. Nevertheless, the impact of LCC on regional surface hydrology is highly relevant to society at large, even when these changes do not impact local or remote atmospheric fields.

Our experiments were designed to place the four forcing scenarios in a common framework. However, there are important differences in the time scales associated with the four scenarios. The SST trend and the LCC pattern both represent longer time-scale processes than the transient signals of an ENSO or an NAO anomaly. The trend anomaly is representative of the century of data (1901–2004) from which the SST forcing patterns were derived. The land cover change scenario is representative of cumulative land cover conversions spread out over several centuries, and our focus of the regional analyses on areas with known LCC may overemphasize the impact of LCC. Despite these differences, the results presented here show that LCC must be accounted for to reliably simulate terrestrial quantities, and they reinforce the need for proper representation of the land surface when considering regional climate.

Although the scale of the SST anomalies in the ENSO and NAO patterns is realistic, it is a simplification to apply these anomalies in the positive phase consistently for many decades. Given the perpetual nature of these anomalies over the 60-yr experiment, we have compared the first 15 yr to the last 15 yr of the WENSO experiment to determine if the experiment can be approximately considered an independent 60-member ensemble of 1-yr ENSO-forced experiments, or whether a cumulative atmospheric response develops wherein precipitation and/or temperature anomalies build up during the course of the experiment. Differenced fields for precipitation and surface air temperature between the start and end of the 60-yr run (not shown) confirm the former, with no significant global or regional-scale coherent differences developing over the course of the

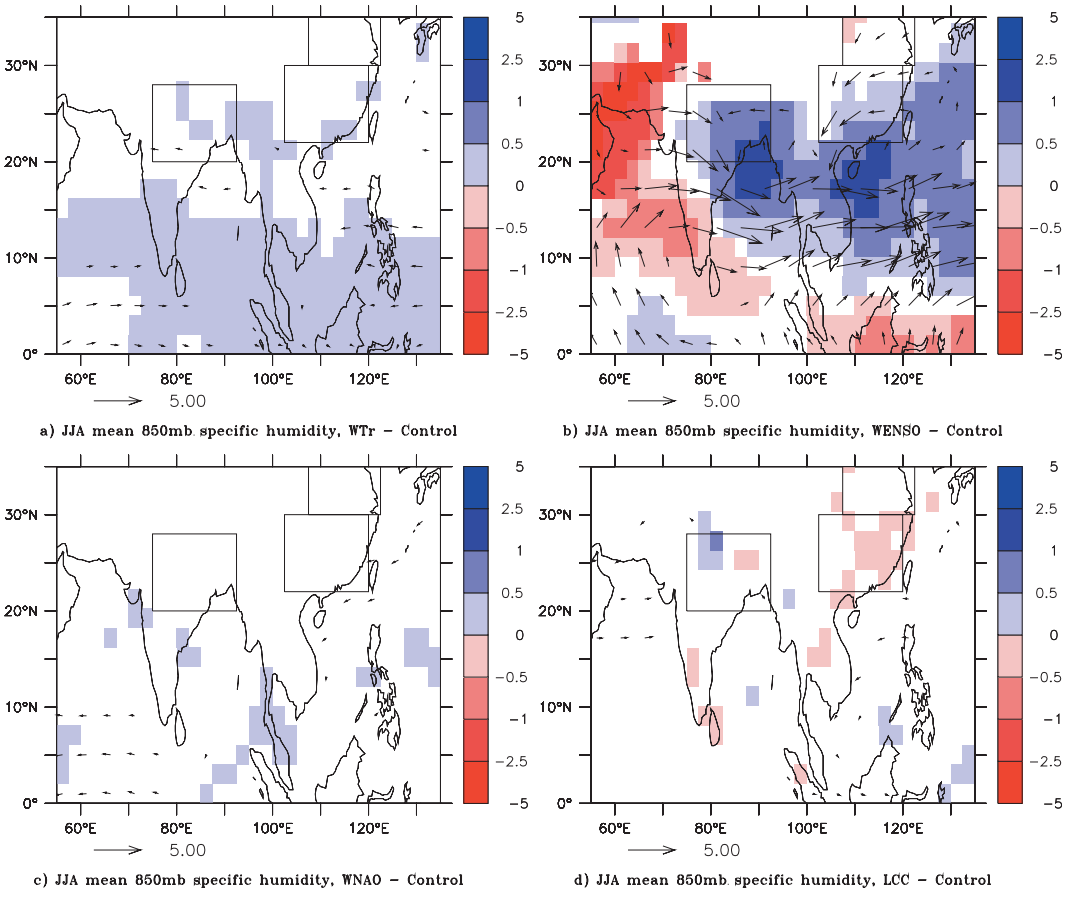

FIG. 11. June–August 850-mb specific humidity differences (color shading; g kg^{-1}) with wind difference overlain. A 5 m s^{-1} scale vector is shown below each plot. (a) WTr − control; (b) WENSO − control; (c) WNAO − control; (d) LCC − control. Specific humidity differences are only shown where they are significant at a 95% level, and winds are only shown when at least one of the components is significantly different at the 95% level. Regions T1, A2, and part of A1 are indicated by black boxes, as in Fig. 2.

experiment. Thus, we can take this experiment to be equivalent to a 60-member ensemble set, consistent with the short intraseasonal time scale for the atmosphere to respond to global SST forcing.

6. Conclusions

Experiments with the atmosphere and land components of the GFDL CM2.1 have been used to compare the relative impacts of anthropogenic land cover conversion (primarily a conversion of forests to grasslands or agriculture) to three realistic SST perturbations: a signal of the global warming SST trend, and two experiments forced by patterns of interannual SST variability (signals similar to warm-phase ENSO and NAO events). The LCC experiment includes biophysical changes resulting from conversion of the vegetation type (changes to the surface albedo, root-zone soil water capacity, stomatal resistance, and roughness length) but does not include impacts on the carbon cycle. Human water-management practices are also not considered in these experiments. Additionally, experimental results are often model dependent, and this study considers output from only one climate model.

Model results show that LCC has a small but significant impact on annual-average global precipitation, evaporation, net radiation, longwave radiation, soil moisture, and runoff. These impacts are largely collocated with regions of land cover disturbance: they do not propagate into the atmosphere to change remote regions, though temperature effects are significant downwind of the altered European region. The SST anomalies, on the other hand, tend to impact a much larger percentage of the globe, with between 30% and 55% of the land surface significantly altered by the warm-phase ENSO perturbation.

In the regions where the land surface is altered, the impact of LCC can be equally or more important than

the SST forcing patterns in determining the seasonal cycle of the surface water and energy balance. Indeed, in many regions, the land cover change experiment had the greatest impact on surface fields such as runoff and soil moisture. In some regions, these fields were significantly affected even when the regional climate was not. Thus, we provide a context for the impacts of LCC on climate: namely, strong regional-scale impacts that can significantly change globally averaged fields but that rarely propagate beyond the disturbed regions. This suggests that LCC must be accounted for to reliably simulate terrestrial quantities over regions of intensive LCC. Furthermore, these results demonstrate that proper representation of the land cover condition is critical in the design of climate model experiments, particularly if those model results are to be used as input to hydrological models and/or higher-resolution climate models, or for regional-scale assessments of climate change or variability.

This points to the need to include significant forcing terms in future climate projections and to the need for a methodology for determining which forcing terms should be included in such climate projections. We suggest that placing any experiment into the context of better-known perturbations may allow for the separation and identification of those processes or parameters that matter in a relative sense. We therefore propose that a set of benchmark simulations be designed to provide the context against which new perturbation experiments can be assessed. This will enable modelers to show that an experiment with any given model produces a regional or global anomaly that is important relative to a known signal. It will also take a small step in dealing with the uncertainty in land surface modeling made apparent by Koster et al. (2006) in their identification of challenges associated with the unknown coupling strength of climate models. We propose experiments to evaluate the relative impacts of three specific perturbations:

1) The impact of a doubling of atmospheric carbon dioxide. This is commonly undertaken and provides a global signal that is societally important and of broad interest.
2) The impact of an ENSO-like SST anomaly. This is a large-scale and recurring SST anomaly that is known to have a globally significant fingerprint.
3) The impact of a LCC anomaly. LCC is highly regionalized and is largely coincident with the distribution of the earth's human population. Such experiments provide a regional pattern of forcing that we have demonstrated to be important for the climate over areas of dense human population. Furthermore, the impact of LCC is highly model dependent, as discussed in the introduction and in Findell et al. (2007).

For a proper assessment of impacts, experiment 1 requires an interactive ocean model (see, e.g., Findell and Delworth 2005), while experiments 2 and 3 can be performed—to first order—with an atmosphere-only model, using fixed SSTs, as in these experiments. Any user-defined anomaly that can be shown to be as globally significant as 1 or 2 is clearly important. However, any user-defined anomaly that impacts those regions of LCC as significantly as LCC itself is also extremely important and worthy of inclusion in models. This would not, of course, be the singular criterion for the relevance of any given forcing. It would, however provide the basis for determining those forcings worthy of immediate attention in coupled climate models.

Acknowledgments. The authors thank Ron Stouffer, Elena Shevliakova, Navin Ramankutty, Richard Betts, and two anonymous reviewers for helpful reviews of the manuscript.

REFERENCES

Avissar, R., and R. A. Pielke, 1989: A parameterization of heterogeneous land surfaces for atmospheric numerical models and its impact on regional meteorology. *Mon. Wea. Rev.,* **117,** 2113–2136.

——, and D. Werth, 2005: Global hydroclimatological teleconnections resulting from tropical deforestation. *J. Hydrometeor.,* **6,** 134–145.

Baede, A. P. M., E. Ahlonsou, Y. Ding, and D. Schimel, 2001: The climate system: An overview. *Climate Change 2001: The Scientific Basis,* J. T. Houghton et al., Eds., Cambridge University Press, 85–98.

Bala, G., K. Caldeira, M. Wickett, T. J. Phillips, D. B. Lobell, C. Delire, and A. Mirin, 2007: Combined climate and carbon-cycle effects of large-scale deforestation. *Proc. Natl. Acad. Sci. USA,* **104,** 6550–6555.

Betts, A. K., J. H. Ball, A. C. M. Beljaars, M. J. Miller, and P. A. Viterbo, 1996: The land surface-atmosphere interaction: A review based on observational and global modeling perspectives. *J. Geophys. Res.,* **101,** 7209–7225.

Betts, R. A., 2000: Offset of the potential carbon sink from boreal forestation by decreases in surface albedo. *Nature,* **408,** 187–190.

——, 2001: Biogeophysical impacts of land use on the present-day climate: Near-surface temperature change and radiative forcing. *Atmos. Sci. Lett.,* **2,** 39–51, doi:10.1006/asle.2001.0037.

——, P. M. Cox, M. Collins, P. P. Harris, C. Huntingford, and C. D. Jones, 2004: The role of ecosystem-atmosphere interactions in simulated Amazonian precipitation decrease and forest dieback under global climate warming. *Theor. Appl. Climatol.,* **78,** 157–175, doi:10.1007/s00704-004-0050-y.

Bonan, G. B., 1999: Frost followed the plow: Impacts of deforestation on the climate of the United States. *Ecol. Appl.,* **94,** 1305–1315.

Bounoua, L., R. Defries, G. J. Collatz, P. Sellers, and H. Khan, 2002: Effects of land cover conversion on surface climate. *Climatic Change,* **52,** 29–64.

Burke, E. J., W. J. Shuttleworth, Z. -L. Yang, S. L. Mullen, and M. A. Arain, 2000: The impact of the parameterization of heterogeneous vegetation on the modeled large-scale circulation in CCM3-BATS. *Geophys. Res. Lett.,* **27,** 397–400.

Chase, T. N., R. A. Pielke Sr., T. G. F. Kittel, J. S. Baron, and T. J. Stohlgren, 1999: Potential impacts on Colorado Rocky Mountains weather due to land use changes on the adjacent Great Plains. *J. Geophys. Res.,* **104,** 16 673–16 690.

——, ——, ——, R. R. Nemani, and S. W. Running, 2000: Simulated impacts of historical land cover changes on global climate in northern winter. *Climate Dyn.,* **16,** 93–105.

Costa, M. H., and J. A. Foley, 2000: Combined effects of deforestation and doubled atmospheric CO_2 concentrations on the climate of Amazonia. *J. Climate,* **13,** 18–34.

Dai, A., and T. M. L. Wigley, 2000: Global patterns of ENSO-induced precipitation. *Geophys. Res. Lett.,* **27,** 1283–1286.

Delworth, T. L., and Coauthors, 2006: GFDL's CM2 global coupled climate models. Part I: Formulation and simulation characteristics. *J. Climate,* **19,** 643–674.

Deser, C., A. Capotondi, R. Saravanan, and A. S. Phillips, 2006: Tropical Pacific and Atlantic climate variability in CCSM3. *J. Climate,* **19,** 2451–2481.

Dickinson, R. E., and A. Henderson-Sellers, 1988: Modelling tropical deforestation: A study of GCM land-surface parameterizations. *Quart. J. Roy. Meteor. Soc.,* **114,** 439–462.

Findell, K. L., and T. L. Delworth, 2005: A modeling study of dynamic and thermodynamic mechanisms for summer drying in response to global warming. *Geophys. Res. Lett.,* **32,** L16702, doi:10.1029/2005GL023414.

——, T. R. Knutson, and P. C. D. Milly, 2006: Weak simulated extratropical responses to complete tropical deforestation. *J. Climate,* **19,** 2835–2850.

——, E. Shevliakova, P. C. D. Milly, and R. J. Stouffer, 2007: Modeled impact of anthropogenic land cover change on climate. *J. Climate,* **20,** 3621–3634.

Forster, P., and Coauthors, 2007: Changes in atmospheric constituents and in radiative forcing. *Climate Change 2007: The Physical Science Basis,* S. Solomon et al., Eds., Cambridge University Press, 129–234.

Gedney, N., and P. J. Valdes, 2000: The effect of Amazonian deforestation on the Northern Hemisphere circulation and climate. *Geophys. Res. Lett.,* **27,** 3053–3056.

GFDL Global Atmospheric Model Development Team, 2004: The new GFDL global atmosphere and land model AM2–LM2: Evaluation with prescribed SST simulations. *J. Climate,* **17,** 4641–4673.

Gibbard, S., K. Caldeira, G. Bala, T. J. Phillips, and M. Wickett, 2005: Climate effects of global land cover change. *Geophys. Res. Lett.,* **32,** L23705, doi:10.1029/2005GL024550.

Goldewijk, K. K., 2001: Estimating global land use change over the past 300 years: The HYDE database. *Global Biogeochem. Cycles,* **15,** 417–433.

Govindasamy, B., P. B. Duffy, and K. Caldeira, 2001: Land use changes and Northern Hemisphere cooling. *Geophys. Res. Lett.,* **28,** 291–294.

Hahmann, A., and R. E. Dickinson, 1997: RCCM2–BATS model over tropical South America: Applications to tropical deforestation. *J. Climate,* **10,** 1944–1964.

Hansen, J. E., M. Sato, A. Lacis, R. Ruedy, I. Tegen, and E. Matthews, 1998: Climate forcings in the industrial era. *Proc. Natl. Acad. Sci. USA,* **95,** 12 753–12 758.

Heck, P., D. Lüthi, H. Wernli, and C. Schär, 2001: Climate impacts of European-scale anthropogenic vegetation changes: A sensitivity study using a regional climate model. *J. Geophys. Res.,* **106,** 7817–7836.

Henderson-Sellers, A., and V. Gornitz, 1984: Possible climatic impacts of land cover transformations, with particular emphasis on tropical deforestation. *Climatic Change,* **6,** 231–257.

Hurtt, G. C., S. Frolking, M. G. Fearon, B. Moore III, E. Shevliakova, S. Malyshev, S. W. Pacala, and R. A. Houghton, 2006: The underpinnings of land-use history: Three centuries of global gridded land-use transitions, wood harvest activity, and resulting secondary lands. *Global Change Biol.,* **12,** 1208–1229.

Kaiser, H. F., 1958: The Varimax criterion for analytic rotations in factor analysis. *Psychometrika,* **23,** 187–200.

Knutson, T. R., and Coauthors, 2006: Assessment of twentieth-century regional surface temperature trends using the GFDL CM2 coupled models. *J. Climate,* **19,** 1624–1651.

Koster, R. D., and Coauthors, 2006: GLACE: The Global Land–Atmosphere Coupling Experiment. Part I: Overview. *J. Hydrometeor.,* **7,** 590–610.

Livezey, R. E., and W. Y. Chen, 1983: Statistical field significance and its determination by Monte Carlo techniques. *Mon. Wea. Rev.,* **111,** 46–59.

Magnusdottir, G., C. Deser, and R. Saravanan, 2004: The effects of North Atlantic SST and sea ice anomalies on the winter circulation in CCM3. Part I: Main features and storm-track characteristics of the response. *J. Climate,* **17,** 857–876.

Mahmood, R., and K. G. Hubbard, 2002: Anthropogenic land-use change in the North American tall grass-short grass transition and modification of near-surface hydrologic cycle. *Climate Res.,* **21,** 83–90.

Matthews, E., 1983: Global vegetation and land use data bases for climate studies. *Bull. Amer. Meteor. Soc.,* **64,** 793–794.

Matthews, H. D., A. J. Weaver, M. Eby, and K. J. Meissner, 2003: Radiative forcing of climate by historical land cover change. *Geophys. Res. Lett.,* **30,** 1055, doi:10.1029/2002GL016098.

McGuffie, K., A. Henderson-Sellers, H. Zhang, T. B. Durbridge, and A. J. Pitman, 1995: Global climate sensitivity to tropical deforestation. *Global Planet. Change,* **10,** 97–128.

Milly, P. C. D., and A. B. Shmakin, 2002: Global modeling of land water and energy balances. Part I: The Land Dynamics (LaD) model. *J. Hydrometeor.,* **3,** 283–299.

Narisma, G. T., and A. J. Pitman, 2003: The impact of 200 years of land cover change on the Australian near-surface climate. *J. Hydrometeor.,* **4,** 424–436.

Pitman, A. J., 2003: The evolution of, and revolution in, land surface schemes designed for climate models. *Int. J. Climatol.,* **23,** 479–510, doi:10.1002/joc.893.

——, and M. Zhao, 2000: The relative impact of observed change in land cover and carbon dioxide as simulated by a climate model. *Geophys. Res. Lett.,* **27,** 1267–1270.

Ramankutty, N., and J. A. Foley, 1999: Estimating historical changes in global land cover: Croplands from 1700 to 1992. *Global Biogeochem. Cycles,* **13,** 997–1027.

Rayner, N. A., D. E. Parker, E. B. Horton, C. K. Folland, L. V. Alexander, D. P. Rowell, E. C. Kent, and A. Kaplan, 2003: Globally complete analyses of sea surface temperature, sea ice, and night marine air temperature since the late nineteenth century. *J. Geophys. Res.,* **108,** 4407, doi:10.1029/2002JD002670.

Sud, Y. C., G. K. Walker, J. -H. Kim, G. E. Liston, P. J. Sellers, and W. K. -M. Lau, 1996: Biogeophysical consequences of a tropical deforestation scenario: A GCM simulation study. *J. Climate,* **9,** 3225–3247.

Thompson, D. W. J., J. J. Kennedy, J. M. Wallace, and P. D. Jones, 2008: A large discontinuity in the mid-twentieth century in observed global-mean surface temperature. *Nature,* **453,** 646–649, doi:10.1038/nature06982.

Twine, T. E., C. J. Kucharik, and J. A. Foley, 2004: Effects of land cover change on the energy and water balance of the Mississippi River basin. *J. Hydrometeor.,* **5,** 640–653.

Van den Dool, H. M., and R. M. Chervin, 1986: A comparison of month-to-month persistence of anomalies in a general circulation model and in the earth's atmosphere. *J. Atmos. Sci.,* **43,** 1454–1466.

Vitousek, P. M., H. A. Mooney, J. Lubchenco, and J. M. Melilo, 1997: Human domination of earth's ecosystems. *Science,* **277,** 494–499.

von Storch, H., and F. W. Zwiers, 1999: *Statistical Analysis in Climate Research*. Cambridge University Press, 484 pp.

Wang, H., A. J. Pitman, M. Zhao, and R. Leeman, 2003: The impact of historical land cover change on the June meteorology of China since 1700 simulated using a regional climate model. *Int. J. Climatol.,* **23,** 511–527.

Wang, X., and S. S. Shen, 1999: Estimation of spatial degrees of freedom of a climate field. *J. Climate,* **12,** 1280–1291.

Werth, D., and R. Avissar, 2002: The local and global effects of Amazon deforestation. *J. Geophys. Res.,* **107,** 8087, doi:10.1029/2001JD000717.

——, and ——, 2005: The local and global effects of African deforestation. *Geophys. Res. Lett.,* **32,** L12704, doi:10.1029/2005GL022969.

Zhang, X., F. W. Zwiers, G. C. Hegerl, F. H. Lambert, N. P. Gillett, S. Solomon, P. A. Stott, and T. Nozawa, 2007: Detection of human influence on twentieth-century precipitation trends. *Nature,* **448,** 461–465, doi:10.1038/nature06025.

Zhao, M., and A. J. Pitman, 2002: The impact of land cover change and increasing carbon dioxide on the extreme and frequency of maximum temperature and convective precipitation. *Geophys. Res. Lett.,* **29,** 1078, doi:10.1029/2001GL013476.

——, ——, and T. N. Chase, 2001: Climatic effects of land cover change at different carbon dioxide levels. *Climate Res.,* **17,** 1–18.

Zwiers, F. W., and H. von Storch, 1995: Taking serial correlation into account in tests of the mean. *J. Climate,* **8,** 336–351.